06

# Structure and dielectric characteristics of $SrTiO_3(111)/Al_2O_3(001)$ films fabricated by RF sputtering

© A.V. Pavlenko,[1] D.V. Stryukov,[1] K.M. Zhidel,[1] Ya.Yu. Matyash,[1] P.A. Shishkina,[2] M.S. Chumak[2]

[1]Federal Research Centre „The Southern Scientific Centre of the Russian Academy of Sciences“,
344006 Rostov-on-Don, Russia
[2]Scientific Research Institute of Physics, Southern Federal University,
344090 Rostov-on-Don, Russia
e-mail: Antvpr@mail.ru

*Received June 20, 2024*
*Revised August 2, 2024*
*Accepted August 15, 2024*

$SrTiO_3$ thin films were grown on an $Al_2O_3(001)$ substrate in an oxygen atmosphere using a one-stage method of high-frequency cathode sputtering of a strontium titanate ceramic target. It is shown that the obtained $SrTiO_3$ films with a thickness of $\sim 120$ nm are single-phase, pure and single-crystalline (surface roughness $\sim 8.5$ nm, lateral size of growth blocks $\sim 100$ nm). The magnitude of the unit cell strain in comparison with the bulk single crystal, the mutual orientations between unit cells of the film and the substrate, as well as the band gap for the direct allowed transition and the indirect one have been established. The dielectric characteristics of the films had been measured, the results of which indicating that the films are in the paraelectric phase at room temperature.

**Keywords:** thin films, dielectric characteristics, heteroepitaxy, STO.

DOI: 10.61011/TP.2024.10.59362.209-24

## Introduction

The applications of ferroelectrics in modern technology range from sensors or various purpose to complex elements of microelectromechanical systems [1]. The trend toward miniaturization of functional elements has steered increasing attention to heterostructures based on thin films [2]. The quality of the film/substrate interface and internal stresses in nanoscale films have a strong influence on the magnitude of polarization, permittivity ($\varepsilon$), and dielectric losses ($\mathrm{tg}\,\delta$) of thin films. Multiferroics based on $BiFeO_3$ [3], high-temperature ferroelectrics based on $Bi_4Ti_3O_{12}$ [4], and quantum ferroelectrics based on $SrTiO_3$ (STO) [5] stand out among the materials that have been studied extensively in recent years. The interest in STO films stems from their high permittivity, which is much needed for integrated capacitors, and their potential applications as a barrier material for reducing leakage currents in heterostructures [6]. At low temperatures, the value of $\varepsilon$ of STO films changes significantly when an electric field is applied, which is of interest for tunable microwave devices operating at cryogenic temperatures. In a stress-free state, strontium titanate is a quantum paraelectric: it remains paraelectric down to 0 K, although chemical [7] or isotopic substitution [8] and the application of electrical voltage disrupt this state easily, inducing ferroelectricity. Specifically, it was demonstrated in [9] that epitaxial strain in STO may raise the Curie temperature by several hundred degrees. Although a significant number of papers focused on establishing the patterns of formation of dielectric and ferroelectric characteristics of thin STO films have already been published, contradictory data on its structure, phase composition, and properties are often found in literature, since they depend on the technique of film fabrication. The present study is concerned with the patterns of formation of the phase composition, crystal structure, and optical and dielectric characteristics of thin STO films grown by RF cathode sputtering in an oxygen atmosphere on single-crystalline $Al_2O_3$ substrates, which, owing to their high electrical resistance ($\sim 10^{-12}\,\Omega\cdot$cm) and low losses in the microwave range, are an excellent substrate for microwave devices. We have found no prior published reports of synthesis of pure STO heteroepitaxial films on single-crystalline $Al_2O_3$ substrates by the indicated method.

## 1. Methods of fabrication and examination of samples

Thin $SrTiO_3$ films with a thickness of $\sim 120$ nm were deposited (the film growth rate was 6 nm/min) onto a single-crystalline $Al_2O_3$ substrate 500 $\mu$m in thickness prepared for heteroepitaxial deposition (cut — 001; double-sided polishing) by RF cathode sputtering in an oxygen atmosphere in one stage. The initial substrate temperature was $\sim 400\,^\circ$C, the pressure of pure oxygen in the chamber was 67 Pa, and the input RF power was 130 W. Since oxygen vacancies are one of the most common defects in oxygen-octahedra materials, the synthesized heterostructure was left in an oxygen atmosphere to cool to room temperature after the deposition was completed. Vertical $Pt/SrTiO_3/Pt/Al_2O_3$ (001) capacitor structures, which allow one to examine the properties of $SrTiO_3$ films in the direction normal to the substrate, were formed for dielectric measurements.

A „RIKOR“ (Cu K$\alpha$ radiation) multifunction X-ray difractometer was used to perform X-ray diffraction analysis (determine the phase composition, structural perfection of the films, unit cell parameters, and orientation relationships between the film and the substrate).

The surface morphology of the polished $Al_2O_3(001)$ substrate and the STO film was investigated with an „Ntegra Academia“ atomic force microscope (AFM) in the semi-contact mode using an NS15/50 (NT-MDT) silicon cantilever. The obtained scans were processed in Image Analysis. Scanning was performed within $1 \times 1\,\mu$m regions with a resolution of $300 \times 300$ points per line; the scan rate was 0.9–1 Hz, and the temperature during scanning was 22 °C.

The optical properties of films were studied with an SF-56 (OKB Spektr, Russia) UV-vis spectrophotometer. Transmittance spectra were recorded within the 190–1100 nm range at room temperature with a scanning step of 1 nm.

A measurement complex with a TF Analyzer 2000 and an MST-4000A probe station was used to measure dielectric hysteresis loops (P(E) dependences) at room temperature.

## 2. Experimental results and discussion

The results of X-ray diffraction analysis of the $STO/Al_2O_3(001)$ heterostructure revealed bright reflections of the STO film and the $Al_2O_3(001)$ substrate only. No traces of impurity phases were found. The $\theta - 2\theta$ X-ray pattern (Fig. 1) for the STO film in the normal scattering geometry features reflections of the $(hhh)_c$ family only, indicating that axis $[111]_c$ is oriented normally to the substrate surface (axis $[001]Al_2O_3$). The STO film and the $Al_2O_3(001)$ substrate interface in the azimuthal plane in directions $[1-10]_c$ and $[-101]_c$, which may be chosen as the basic directions for analysis in the hexagonal approximation. However, we use the pseudo-cubic approximation for convenience; its reflections and directions are marked with subscript „c.“ The obtained thin STO film is epitaxial, which

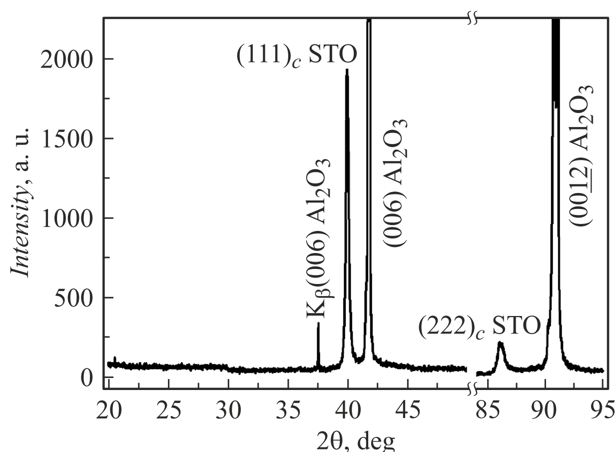


**Figure 1.** $\theta - 2\theta$ X-ray pattern of an $STO/Al_2O_3(001)$ thin film in the normal scattering geometry.

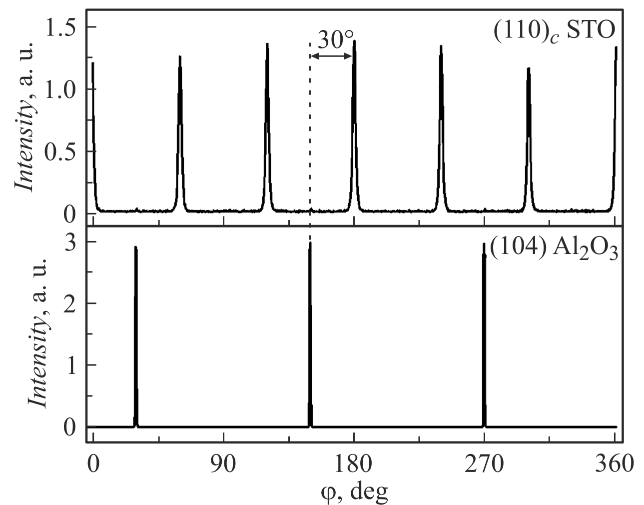


**Figure 2.** X-ray patterns of $\varphi$-scans of reflections $(110)_c$ of the STO layer and (104) of the $Al_2O_3$ substrate for an $STO/Al_2O_3(001)$ thin film.

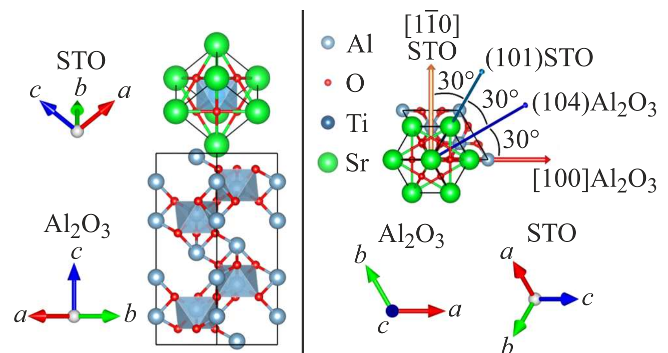


**Figure 3.** Model of mutual orientation of unit cells of the STO film and the $Al_2O_3$ substrate.

is evidenced by six bright maxima in the $\varphi$-scans of the $(110)_c$ reflection (Fig. 2). A comparison of their angular positions with the positions of reflection $(104)Al_2O_3$ revealed a 30° shift, which corresponds to the misorientation of axis $[1-10]_c$ of the STO film relative to axis $[100]Al_2O_3$. The schematic diagram of mutual orientation of the STO film and the $Al_2O_3$ substrate is shown in Fig. 3.

The $\theta - 2\theta$ X-ray patterns of reflections $(110)_c$ were measured to determine the unit cell distortion. A 60° rotation in $\varphi$ does not alter the angular position of the maximum in these patterns (Fig. 4, *a*).

Thus, a cubic cell with parameter $a = 3.912 \pm 0.002$ Å fits all the obtained X-ray patterns (in both symmetric and asymmetric scattering geometries). The obtained parameter is only slightly larger than the parameter of bulk STO ($a_{\text{bulk}} = 3.905$ Å) and corresponds to a tensile strain of unit cell (below 0.2%). The FWHM values of reflections in rocking curves (Fig. 4, *b*) and $\varphi$-scans (Fig. 2) were used to determine the vertical and azimuthal misorientations (1.4° and 2.5°, respectively). Coupled

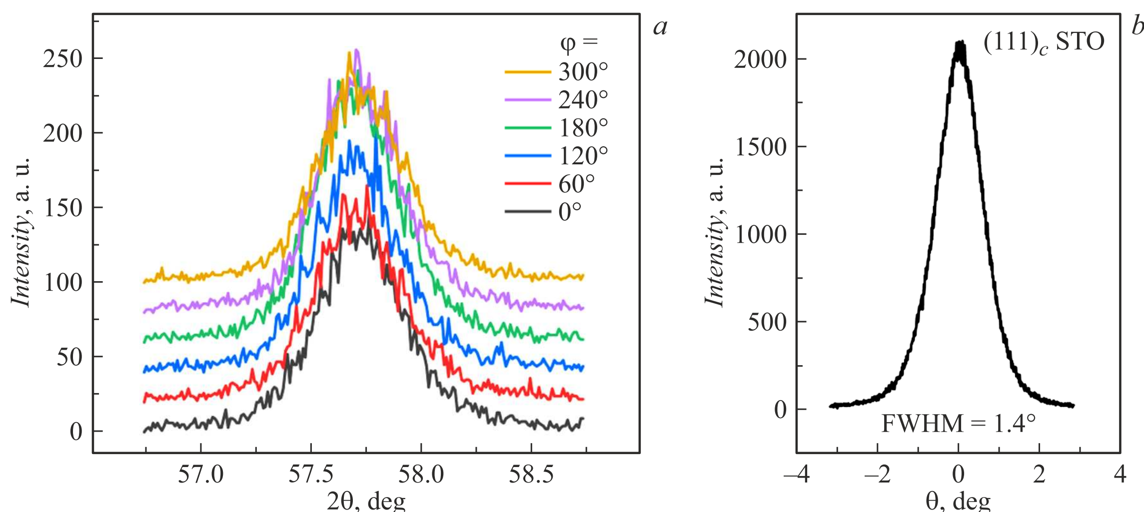


**Figure 4.** *a* — $\theta - 2\theta$ X-ray patterns of $(110)_c$ reflections with rotation in $\varphi$ in $60^\circ$ steps in the asymmetric scattering geometry for $STO/Al_2O_3(001)$; *b* — rocking curve of reflection $(111)_c$ of the STO layer.

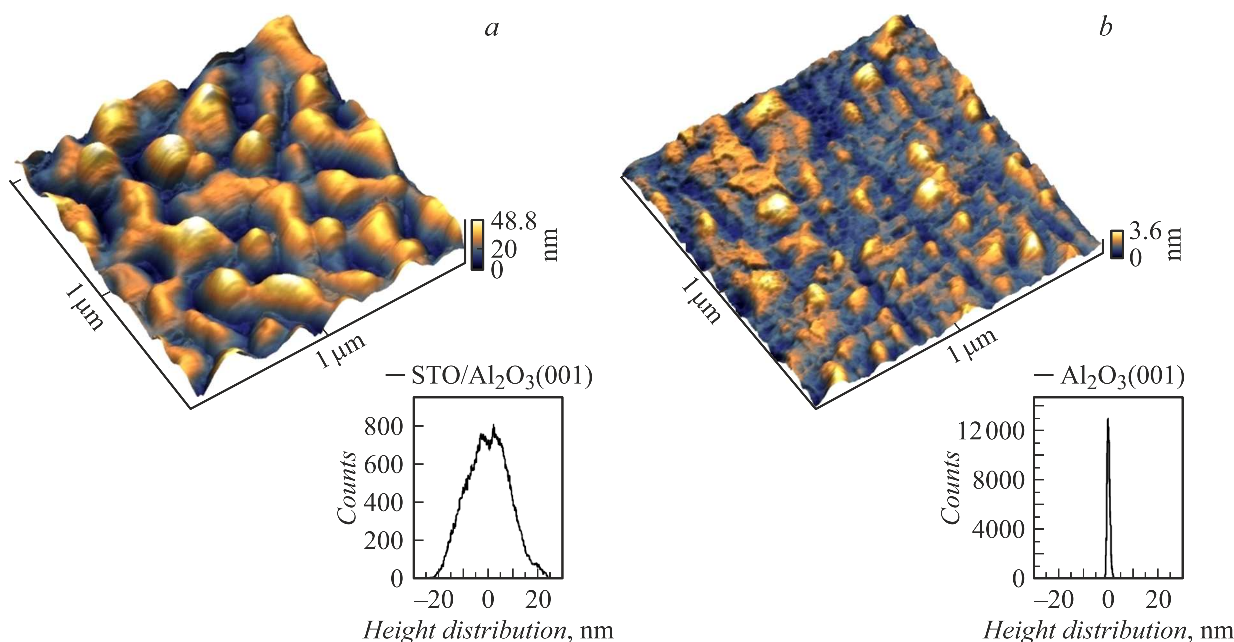


**Figure 5.** Three-dimensional image of a $1 \times 1\,\mu m^2$ surface fragment of the $STO/Al_2O_3(001)$ film (*a*) and the $Al_2O_3(001)$ substrate (*b*); histograms of height distributions for the film and substrate surfaces are shown in the corresponding insets.

with small FWHM values of reflections corresponding to the STO layer in all the obtained X-ray patterns ($\theta - 2\theta$, $\varphi$, and rocking curves), these modest axial misorientations are indicative of a high degree of structural perfection of the obtained thin STO film, which was also manifested in the study of its nanostructure and optical properties. The synthesis of thin STO films with a small unit cell strain should have a positive effect on dielectric characteristics, since it has already been demonstrated that an increased strain may lead to a reduction in permittivity and exert a negative influence on tunability [10].

Figure 5 illustrates the topography of the STO film $\sim 120$ nm in thickness and the $Al_2O_3(001)$ substrate. It can be seen that the film surface does not contain pores, cavities, or other growth defects and is formed by visually identifiable growth blocks of both round and oblong shapes with smoothed boundaries.

In addition, one may notice the interfaces of these blocks, the lateral size of which ($\sim 100$ nm) was calculated using the watershed method. The root-mean-square surface roughness of the obtained STO film was $\sim 8.5$ nm (see the inset in Fig. 5). With the X-ray diffraction data for the $STO/Al_2O_3(001)$ heterostructure taken into account, the

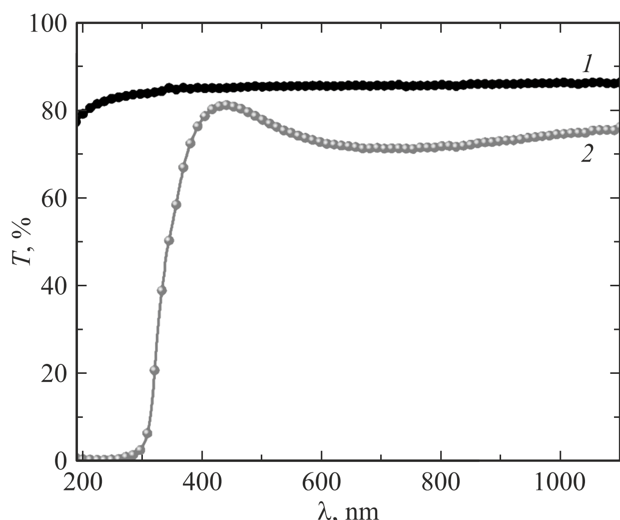


**Figure 6.** Transmittance spectra $T(\lambda)$: *1* — $Al_2O_3$ substrate, *2* — $STO/Al_2O_3(001)$ film.

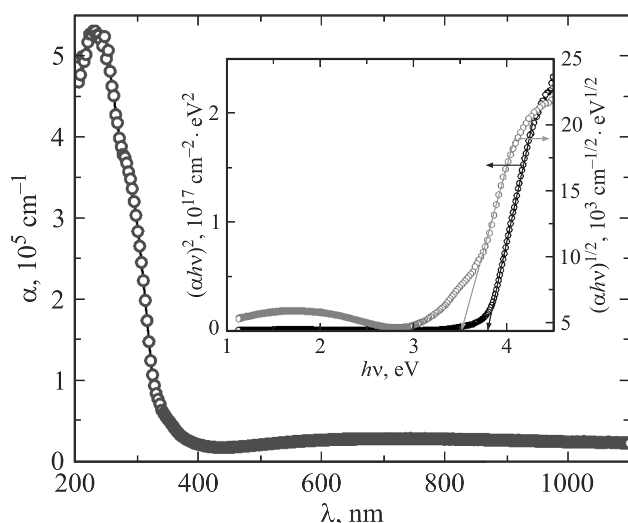


**Figure 7.** Absorption spectrum $\alpha(\lambda)$ of the $STO/Al_2O_3(001)$ film. Dependences $(\alpha h\nu)^2$ and $(\alpha h\nu)^{1/2}$ vs. $h\nu$ for the $STO/Al_2O_3(001)$ film are shown in the inset.

island growth mechanism [11], which produces a surface with these distinct features, appears to be the most probable in the case of the strontium titanate film. In the island mechanism, small nuclei emerge directly on the substrate surface and then grow in size, turning into large condensed-phase islands that merge and eventually form a continuous film [12,13].

The STO film on the sapphire substrate is characterized by a fairly high transparency ($T = 71-81\%$) within the wavelength range from 400 to 1100 nm and a sharp reduction in transmittance in the UV region (Fig. 6). Compared to the transmittance of the $Al_2O_3$ substrate ($T = 85\%$), the optical transmittance of the film is indicative of its homogeneity.

Figure 7 presents absorption spectrum $\alpha(\lambda)$ of the $STO/Al_2O_3(001)$ film. Absorption coefficient $\alpha$ was calculated in accordance with the Lambert–Beer law:

$$\alpha = (1/d)\ln(1/T),$$

where $d$ is the film thickness.

It can be seen that absorption coefficient $\alpha$ increases steadily with decreasing wavelength and starts increasing rapidly at $\lambda < 350$ nm. It is known [14–18] that fundamental optical transitions in strontium titanate include both direct and indirect ones. In view of this, the region with a high observed absorption coefficient was analyzed using the ratio

$$\alpha h\nu = \text{const}(h\nu - E_g)^m,$$

where power exponent $m$ specifies the optical transition type (its values of 0.5 and 2 correspond to direct and indirect allowed transitions, respectively); const is a frequency-independent parameter; $h$ is the Planck constant; $\nu$ is the photon frequency; and $E_g$ is the band gap.

Following [15–17], we extrapolated straight-line sections of the dependences of $(\alpha h\nu)^2$ and $(\alpha h\nu)^{1/2}$ on the photon energy to the abscissa axis (inset in Fig. 7) to determine the band gap. The band gap was thus estimated for the $STO/Al_2O_3(001)$ film: $\sim 3.78$ eV for the direct allowed transition and 3.34 eV for the indirect one. If one takes into account the specifics of the used method, which is less accurate than spectral ellipsometry [19] and the method of two-photon absorption [20,21], the obtained results agree fairly well with the experimental data for the STO single crystal presented in [17], where the indirect and direct band gap energies were found to be equal to 3.25 and 3.75 eV, respectively. However, according to results reported in [19,22], tensile strain should induce a shift of the band edge toward lower energies. A similar widening of the band gap under tensile strain ($\sim 2.2\%$) of the unit cell has already been observed in STO films on $KTaO_3$ substrates and was tentatively associated with the emergence of a polar phase. Similar processes are likely to occur in the present case.

Figure 8 shows a family of dielectric hysteresis loops for the $Pt/STO/Pt(111)/Al_2O_3(001)$ heterostructure measured at room temperature. In weak fields, the $P(E)$ dependence is almost linear (this is also evident from the $P_{\max}(E)$ dependence), which is typical of materials of this kind in the paraelectric phase. Notably, the STO film was characterized by fairly high values of $\varepsilon$ (more than 700) and low $\operatorname{tg}\delta$ (below 0.01) at alternating electric field frequencies of $10^3-10^6$ Hz. As the electric field strength increased, a fairly narrow loop in the $P(E)$dependence formed gradually with the following parameters at $E = 520$ kV/cm: maximum polarization was 36.2 $\mu$C/cm$^2$; residual polarization was 7.47 $\mu$C/cm$^2$; coercive field was 37.8 kV/cm. Within the analyzed range of $E$ values, the $Pt/STO/Pt(111)/Al_2O_3(001)$ structure relaxed rapidly to the initial unpolarized state after the completion of the field application cycle. This suggests that a polar state is induced in the STO film when an electric field is applied. This state is unstable in zero field, which

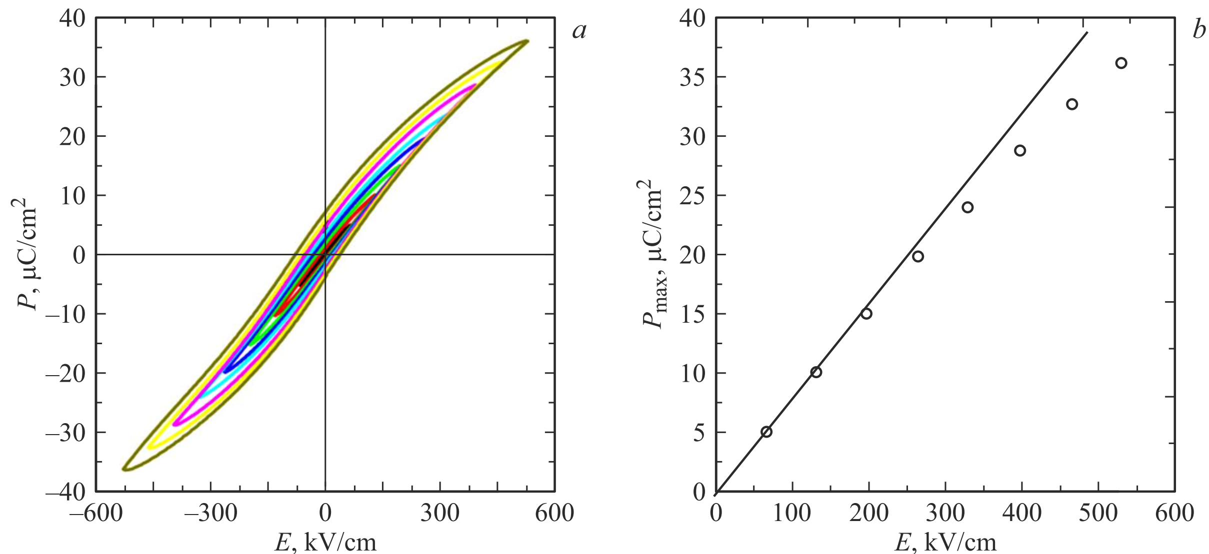


**Figure 8.** Dependences $P(E)$ for the $Pt/STO/Pt(111)/Al_2O_3(001)$ heterostructure at $f = 1$ kHz.

needs to be taken into account in the process of fabrication of multilayer structures based on STO films.

We would like to note the following. Thin films of strontium titanate may grow in different crystallographic directions on the surface of an $Al_2O_3(001)$ single crystal, and the coexistence of different crystallographic orientations has been noted numerous times [23–25]. It was found in [10] that, depending on the substrate temperature, STO films synthesized on $Al_2O_3(001)$ by RF magnetron sputtering are either highly disordered and (110)-oriented or characterized by the coexistence of orientations (110) and (111). Our preliminary studies have demonstrated that a 10% reduction in RF power in the used growth process may lead to texturing of STO films: in addition to the $(hhh)_c$ lines, $(00l)_c$ lines emerged in the $\theta - 2\theta$ X-ray patterns. This makes it impossible to use STO films efficiently as a sublayer in multilayer heterostructures (specifically, in combination with $BiFeO_3$ and $NaNbO_3$).

## 3. Findings and conclusion

1. Heteroepitaxial impurity-free $SrTiO_3$ films $\sim 120$ nm in thickness were synthesized by RF cathode sputtering on an $Al_2O_3(001)$ substrate. The results of X-ray diffraction analysis revealed that the unit cell of $SrTiO_3$ has, as in the bulk material, cubic symmetry and is characterized by an insignificant strain, which does not exceed 0.2%. These cells are oriented in such a way that axis [111] of $SrTiO_3$ is parallel to axis [001] of the substrate and axis $[1{-}10]_c$ of $SrTiO_3$ is rotated by 30° relative to axis [100] of the substrate.

2. AFM studies of the nanostructure of the obtained objects demonstrated that the film surface is homogeneous; does not contain inclusions, pores, or other growth defects; and is characterized by a roughness of $\sim 8.5$ nm and a lateral size of growth blocks of $\sim 100$ nm.

3. Analysis of the optical transmittance spectra of the $STO/Al_2O_3(001)$ heterostructure revealed that the STO film is highly transparent ($T = 71 - 81\%$) within the wavelength range from 400 to 1100 nm, but its transmittance decreases sharply in the UV region; at room temperature, the band gap for direct and indirect allowed transitions is $\sim 3.78$ and $\sim 3.34$ eV, respectively.

4. It was found that the STO film is in a paraelectric state with high values of $\varepsilon$ (more than 700) and low $\mathrm{tg}\,\delta$ (below 0.01) at $f = 10^3 - 10^6$ Hz and room temperature. The application of a strong electric field leads to the formation of a polar state (dependences $P(E)$ take the form of hysteresis loops, at $E = 520$ kV/cm: $P_{max} = 36.2\,\mu C/cm^2$, $P_R = 7.47\,\mu C/cm^2$, and $E_C = 37.8$ kV/cm), which is unstable in zero field.

### Funding

This paper was prepared under the state assignment of the Southern Scientific Centre of the Russian Academy of Sciences (state registration number of the project: 122020100294-9).

### Conflict of interest

The authors declare that they have no conflict of interest

## References

[1] L.W. Martin, A.M. Rappe. Nat. Rev. Mater., **2**, 16087 (2016). DOI: 10.1038/natrevmats.2016.87
[2] K. Yao, S. Chen, S.C. Lai, Y.M. Yousry. Adv. Sci., **9**, 2103842 (2022). DOI: 10.1002/advs.202103842
[3] M. Botea, C. Chirila, G.A. Boni, I. Pasuk, L. Trupina, I. Pintilie, L.M. Hrib, B. Nicu, L. Pintilie. Electron. Mater., **3** (2), 173 (2022). DOI: 10.3390/electronicmat3020015

[4] A.S. Anokhin, S.V. Biryukov, Yu.I. Golovko, V.M. Mukhortov. Nauka Yuga Ross., **14** (1), 29 (2018) (in Russian). DOI: 10.23885/2500-0640-2018-14-1-29-34
[5] A. Baki, M. Abdeldayem, C. Morales, J.I. Flege, D. Klimm, O. Bierwagen, J. Schwarzkopf. Crystal Growth & Design., **23** (4), 2522 (2023). DOI: 10.1021/acs.cgd.2c01438
[6] V.A. Gritsenko, D.R. Islamov. *Fizika dielektricheskikh plenok: mekhanizmy transporta zaryada i fizicheskie osnovy priborov pamyati* (Parallel', Novosibirsk, 2017) (in Russian).
[7] C. Ang, Z. Yu, P.M. Vilarinho, J.L. Baptista. Phys. Rev. B, **57** (13), 7403 (1998). DOI: 10.1103/PhysRevB.57.7403
[8] M. Itoh, R. Wang. Appl. Phys. Lett., **76** (2), 221 (2000). DOI: 10.1063/1.125708
[9] J.H. Haeni, P. Irvin, W. Chang, R. Uecker, P. Reiche, Y.L. Li, S. Choudhury, W. Tian, M.E. Hawley, B. Craigo, A.K. Tagantsev, X.Q. Pan, S.K. Streiffer, L.Q. Chen, S.W. Kirchoefer, J. Levy, D.G. Schlom. Nature, **430**, 758 (2004). DOI: 10.1038/nature02773
[10] R. Wördenweber, E. Hollmann, R. Ott, T. Hürtgen, T.K. Lee. J. Electroceram., **22**, 363 (2009). DOI: 10.1007/s10832-007-9399-5
[11] S.A. Kukushkin, A.V. Osipov. Phys.-Usp., **41**, 983 (1998). DOI: 10.1070/PU1998v041n10ABEH000461
[12] A. Venables, G.D.T. Spiller, M. Hanbucken. Rep. Prog. Phys., **47**, 399 (1984). DOI: 10.1088/0034-4885/47/4/002
[13] D.W. Pashley. Adv. Phys., **14**, 327 (1965). DOI: 10.1080/00018736500101071
[14] S. Zollner, A.A. Demkov, R. Liu, P.L. Fejes, R.B. Gregory, P. Alluri, J.A. Curless, Z. Yu, J. Ramdani, R. Droopad, T.E. Tiwald, J.N. Hilfiker, J.A. Woollam. J. Vac. Sci. Technol. B, **18** (4), 2242 (2000). DOI: 10.1116/1.1303741
[15] C.-H. Lee, N.J. Podraza, Y. Zhu, R.F. Berger, S. Shen, M. Sestak, R.W. Collins, L.F. Kourkoutis, J.A. Mundy, H. Wang, Q. Mao, X. Xi, L.J. Brillson, J.B. Neaton, D.A. Muller, D.G. Schlom. Appl. Phys. Lett., **102**, (12), 122901 (2013). DOI: 10.1063/1.4798241
[16] V. Roge, C. Garlisi, P.L. Popa, K. Menguelti, M. Michel, C. Vergne, E. Wagner, W. Maudez, G. Benvenuti, B.R. Pistillo, E. Barborini. J. Mater. Chem. A, (2024). DOI: 10.1039/D3TA07695D
[17] Y. Gao, Y. Masuda, K. Koumoto. J. Korean Ceramic Society, **40** (3), 213 (2003). DOI: 10.4191/kcers.2003.40.3.213
[18] K. Benthem, C. Elsässer, R.H. French. J. Appl. Phys., **90** (12), 6156 (2001). DOI: 10.1063/1.1415766
[19] A. Dejneka, M. Tyunina, J. Narkilahti, J. Levoska, D. Chvostova, L. Jastrabik, V.A. Trepakov. Physics of the Solid State, **52** (10), 1943 (2010).
[20] S.I. Shablaev, A.M. Danishevskii, V.K. Subashiev, A.A. Babashkin, Fiz. Tverd. Tela, **21**, 1140 (1979) (in Russian).
[21] S.I. Shablaev, A.M. Danishevskii, V.K. Subashiev. J. Exp. Theor. Phys., **59**, 1256 (1984).
[22] T.S. Narasimhamurty. *Photoelastic and Electrooptic Properties of Crystals* (Plenum Press, NY.-London, 1981)
[23] D.O. Klenov, T.R. Taylor, S. Stemmer. J. Mater. Res., **19** (5), 1477 (2004). DOI: 10.1557/JMR.2004.0197
[24] T.R. Taylor, P.J. Hansen, N. Pervez, B. Acikel, R.A. York, J.S. Speck. J. Appl. Phys., **94** (5), 3390 (2003). DOI: 10.1063/1.1598274
[25] G. Panomsuwan, O. Takai, N. Saito. Appl. Surf. Sci., **309**, 95 (2014). DOI: 10.1016/j.apsusc.2014.04.186

*Translated by D.Safin*